

Christeson, G.L., Gulick, S.P.S., Morgan, J.V., Gebhardt, C., Kring, D.A., Le Ber, E., Lofi, J., Nixon, C., Poelchau, M., Rae, A.S.P., Rebolledo-Vieyra, M., Riller, U., Schmitt, D.R., Wittmann, A., Bralower, T.J., Chenot, E., Claeys, P., Cockell, C.S., Coolen, M.J.L., Ferrière, L., Green, S., Goto, K., Jones, H., Lowery, C.M., Mellett, C., Ocampo-Torres, R., Perez-Cruz, L., Pickersgill, A.E., Rasmussen, C., Sato, H., Smit, J., Tikoo, S.M., Tomioka, N., Urrutia-Fucugauchi, J., Whalen, M.T., Xiao, L., and Yamaguchi, K.E. (2018) Extraordinary rocks from the peak ring of the Chicxulub impact crater: P-wave velocity, density, and porosity measurements from IODP/ICDP Expedition 364. *Earth and Planetary Science Letters*, 495, pp. 1-11.

There may be differences between this version and the published version. You are advised to consult the publisher's version if you wish to cite from it.

<http://eprints.gla.ac.uk/163984/>

Deposited on: 20 July 2018

# ***Extraordinary Rocks from the Peak Ring of the Chicxulub Impact Crater: P-Wave Velocity, Density, and Porosity Measurements from IODP/ICDP Expedition 364***

**G.L. Christeson<sup>1</sup>, S.P.S. Gulick<sup>1,2</sup>, J.V. Morgan<sup>3</sup>, C. Gebhardt<sup>4</sup>, D.A. Kring<sup>5</sup>, E. Le Ber<sup>6</sup>, J. Lofi<sup>7</sup>, C. Nixon<sup>8</sup>, M. Poelchau<sup>9</sup>, A.S.P. Rae<sup>3</sup>, M. Rebolledo-Vieyra<sup>10</sup>, U. Riller<sup>11</sup>, D.R. Schmitt<sup>8,12</sup>, A. Wittmann<sup>13</sup>, T.J. Bralower<sup>14</sup>, E. Chenot<sup>15</sup>, P. Claeys<sup>16</sup>, C.S. Cockell<sup>17</sup>, M.J.L. Coolen<sup>18</sup>, L. Ferrière<sup>19</sup>, S. Green<sup>20</sup>, K. Goto<sup>21</sup>, H. Jones<sup>14</sup>, C.M. Lowery<sup>1</sup>, C. Mellett<sup>22</sup>, R. Ocampo-Torres<sup>23</sup>, L. Perez-Cruz<sup>24</sup>, A.E. Pickersgill<sup>25,26</sup>, C. Rasmussen<sup>27,28</sup>, H. Sato<sup>29,30</sup>, J. Smit<sup>31</sup>, S.M. Tikoo<sup>32</sup>, N. Tomioka<sup>33</sup>, J. Urrutia-Fucugauchi<sup>24</sup>, M.T. Whalen<sup>34</sup>, L. Xiao<sup>35</sup>, and K.E. Yamaguchi<sup>36,37</sup>**

<sup>1</sup>University of Texas Institute for Geophysics, Jackson School of Geosciences, Austin, USA

<sup>2</sup>Department of Geological Sciences, Jackson School of Geosciences, Austin, USA

<sup>3</sup>Department of Earth Science and Engineering, Imperial College, London, UK

<sup>4</sup>Alfred Wegener Institute Helmholtz Centre of Polar and Marine Research, Bremerhaven, Germany

<sup>5</sup>Lunar and Planetary Institute, Houston, USA

<sup>6</sup>Department of Geology, University of Leicester, UK

<sup>7</sup>Géosciences Montpellier, Université de Montpellier, France

<sup>8</sup>Department of Physics, University of Alberta, Canada

<sup>9</sup>Department of Geology, University of Freiburg, Germany

<sup>10</sup>SM 312, Mza 7, Chipre 5, Resid. Isla Azul, Cancun, Quintana Roo, Mexico

<sup>11</sup>Institut für Geologie, Universität Hamburg, Germany

<sup>12</sup>Now at Department of Earth, Atmospheric, and Planetary Sciences, Purdue University, USA

<sup>13</sup>Eyring Materials Center, Arizona State University, Tempe, USA

<sup>14</sup>Department of Geosciences, Pennsylvania State University, University Park, USA

<sup>15</sup>Biogéosciences Laboratory, Université de Bourgogne-Franche Comté, France

<sup>16</sup>Analytical, Environmental and Geo-Chemistry, Vrije Universiteit Brussel, Brussels, Belgium

<sup>17</sup>School of Physics and Astronomy, University of Edinburgh, UK

<sup>18</sup>Department of Chemistry, WA-Organic and Isotope Geochemistry Centre (WA-OIGC), Curtin University, Bentley, Australia

<sup>19</sup>Natural History Museum, Vienna, Austria

<sup>20</sup>British Geological Survey, Edinburgh, UK

<sup>21</sup>International Research Institute of Disaster Science, Tohoku University, Sendai, Japan

<sup>22</sup>United Kingdom Hydrographic Office, Taunton, UK

- <sup>23</sup>Groupe de Physico-Chimie de l'Atmosphère, L'Institut de Chimie et Procédés pour l'Énergie, l'Environnement et la Santé (ICPEES), Université de Strasbourg, France
- <sup>24</sup>Instituto de Geofísica, Universidad Nacional Autónoma De México, Ciudad de México, México
- <sup>25</sup>School of Geographical and Earth Sciences, University of Glasgow, UK
- <sup>26</sup>Argon Isotope Facility, Scottish Universities Environmental Research Centre (SUERC), East Kilbride, UK
- <sup>27</sup>Department of Geology and Geophysics, University of Utah, Salt Lake City, USA
- <sup>28</sup>Now at University of Texas Institute for Geophysics, Jackson School of Geosciences, Austin, USA
- <sup>29</sup>Japan Agency for Marine-Earth Science and Technology, Kanagawa, Japan
- <sup>30</sup>Now at Ocean Resources Research Center for Next Generation, Chiba Institute of Technology, Chiba, Japan
- <sup>31</sup>Faculty of Earth and Life Sciences (FALW), Vrije Universiteit Amsterdam, Netherlands
- <sup>32</sup>Earth and Planetary Sciences, Rutgers University New Brunswick, USA
- <sup>33</sup>Kochi Institute for Core Sample Research, Japan Agency for Marine-Earth Science and Technology, Kochi, Japan
- <sup>34</sup>Department of Geosciences, University of Alaska Fairbanks, USA
- <sup>35</sup>School of Earth Sciences, Planetary Science Institute, China University of Geosciences (Wuhan), China
- <sup>36</sup>Department of Chemistry, Toho University, Chiba, Japan
- <sup>37</sup>NASA Astrobiology Institute

Corresponding author:

Gail L Christeson

University of Texas Institute for Geophysics

Jackson School of Geosciences

J.J. Pickle Research Campus, Mail Code R2200

10100 Burnet Rd, Austin, Texas 78758

(512)471-0463

[gail@ig.utexas.edu](mailto:gail@ig.utexas.edu)

1

2

Revised for EPSL April 4, 2018

3

## Highlights

- Chicxulub peak-ring rocks have low velocities and densities, and high porosities.
- Physical property values indicate considerable damage of granitoid peak-ring rocks.
- Suevite flowed downslope during and after peak-ring formation

**Abstract.** Joint International Ocean Discovery Program and International Continental Scientific Drilling Program Expedition 364 drilled into the peak ring of the Chicxulub impact crater. We present P-wave velocity, density, and porosity measurements from Hole M0077A that reveal unusual physical properties of the peak-ring rocks. Across the boundary between post-impact sedimentary rock and suevite (impact melt-bearing breccia) we measure a sharp decrease in velocity and density, and an increase in porosity. Velocity, density, and porosity values for the suevite are 2900-3700 m/s, 2.06-2.37 g/cm<sup>3</sup>, and 20-35%, respectively. The thin (25 m) impact melt rock unit below the suevite has velocity measurements of 3650-4350 m/s, density measurements of 2.26-2.37 g/cm<sup>3</sup>, and porosity measurements of 19-22%. We associate the low velocity, low density, and high porosity of suevite and impact melt rock with rapid emplacement, hydrothermal alteration products, and observations of pore space, vugs, and vesicles. The uplifted granitic peak ring materials have values of 4000-4200 m/s, 2.39-2.44 g/cm<sup>3</sup>, and 8-13% for velocity, density, and porosity, respectively; these values differ significantly from typical unaltered granite which has higher velocity and density, and lower porosity. The majority of Hole M0077A peak-ring velocity, density, and porosity measurements indicate considerable rock damage, and are consistent with numerical model predictions for peak-ring formation where the lithologies present within the peak ring represent some of the most shocked and damaged rocks in an impact basin. We integrate our results with previous seismic datasets to map the suevite near the borehole. We map suevite below the Paleogene sedimentary rock in the annular trough, on the peak ring, and in the central basin, implying that, post impact, suevite covered the entire floor of the impact basin. Suevite thickness is 100-165 m on the top of the peak ring but 200 m in

the central basin, suggesting that suevite flowed downslope from the collapsing central uplift during and after peak-ring formation, accumulating preferentially within the central basin.

**Keywords.** Chicxulub, peak ring, physical properties, impact crater

## 1. Introduction

Present in the two largest classes of impact craters, peak-ring craters and multi-ring basins, peak rings are interpreted to develop from gravitational collapse of a central peak, and exhibit a circular ring of elevated topography interior of the crater rim [e.g., *Grieve et al.*, 1981; *Morgan et al.*, 2016]. Surface topography can be observed for craters on the Moon and other rocky planets, but on Earth craters can also be characterized at depth by boreholes and geophysical studies. The Chicxulub impact crater is the only known terrestrial crater that preserves an unequivocal peak ring [e.g., *Morgan et al.*, 1997; *Morgan et al.*, 2000], and can provide important information related to peak-ring formation with implication for how impacts act as a geologic process on planetary surfaces.

The Chicxulub peak ring has been imaged by a grid of seismic reflection profiles (Figure 1), which constrain a morphological feature that rises ~0.2-0.6 km above the floor of the central basin and annular trough and is overlain by ~0.6-1.0 km of post-impact sedimentary rock [*Morgan et al.*, 1997; *Gulick et al.*, 2008; *Gulick et al.*, 2013] (Figure 2b). Tomographic velocity images associate the uppermost 0.1-0.2 km of the peak ring with low seismic velocities (Figure 2), which were interpreted as a thin layer of highly porous allogenic impact breccias [*Morgan et al.*, 2011]. Velocities 0.5-2.5 km beneath the peak-ring surface are reduced compared to adjacent material in the annular trough and central basin [*Morgan et al.*, 2000; *Morgan et al.*, 2002], and were interpreted as highly-fractured basement rocks [*Morgan et al.*, 2000], as predicted by numerical simulations of peak-ring formation [e.g., *Collins et al.*, 2008].

The International Ocean Discovery Program and International Continental Scientific Drilling Program (IODP/ICDP) Expedition 364 drilled and cored the Chicxulub peak ring and overlying post-impact sedimentary rock from depths 505.7-1334.7 m below the seafloor (mbsf) [*Morgan et*

*al.*, 2017]. Hole M0077A (Figure 1) provides the ground-truth information calibrating our geophysical data and interpretations. Here we report the first P-wave velocity, density, and porosity measurements of the Chicxulub peak ring at scales ranging from centimeters to meters. We combine these results with existing geophysical data to gain insight into deposition of suevite (impact melt-bearing breccia [Stöffler and Grieve, 2007]) and impact melt rock (crystalline rock solidified from impact melt [Stöffler and Grieve, 2007]), and into the physical state of the peak-ring rocks.

## **2. Datasets**

### **2.1. Surface Seismic Surveys**

Deep-penetration seismic reflection surveys that image the Chicxulub impact crater were acquired in 1996 [Morgan *et al.*, 1997] and 2005 [Gulick *et al.*, 2008]. These data include regional profiles and a grid over the northwest peak-ring region. Air gun shots fired for these two surveys were also recorded by ocean bottom and land seismometers (Figure 1). The seismic reflection images are most recently summarized in Gulick *et al.* [2013]. Morgan *et al.* [2011] used wide-angle seismic data recorded on the 6-km seismic reflection hydrophone cable (streamer) to produce high-resolution full-waveform inversion (FWI) velocity models of the shallow crust. The surface seismic data predicted the top of the peak ring at Hole M0077A at 650 mbsf (Figure 2b).

In this study we focus on comparisons of Expedition 364 results with seismic reflection images and FWI velocity models. Vertical resolution in seismic reflection images (Figure 2b) at the top of the peak ring is ~35-40 m (one quarter of the ~150-m seismic wavelength [e.g., Yilmaz, 1987] for a frequency of 20 Hz and velocity of 3000 m/s, which is the average P-wave velocity in the suevite). Spatial resolution for FWI velocity models at the top of the peak ring (Figure 2a) is ~150-m (half the ~300-m seismic wavelength [Virieux and Operto, 2009] for the highest FWI frequency of 10 Hz and velocity of 3000 m/s [Morgan *et al.*, 2011]).

## 2.2. Core Measurements

P-wave and Moisture and Density (MAD) measurements were made on sample plugs with average volumes of  $\sim 6 \text{ cm}^3$  at  $\sim 1 \text{ m}$  spacing throughout all the cores. P-wave velocities were measured using a source frequency of 250 kHz (wavelength of  $\sim 1 \text{ cm}$  at 3000 m/s), and have an estimated uncertainty of  $\sim 125 \text{ m/s}$  based on the standard deviation between repeat measurements on a subset of samples. MAD procedures included obtaining wet and dry sample weights and dry sample volume; these values allowed computation of bulk density and porosity. Weights and volumes were obtained to a precision of 0.0001 g and  $0.04 \text{ cm}^3$ , respectively, which result in estimated uncertainties for bulk densities of  $\sim 0.006 \text{ g/cm}^3$  and porosities of  $< 0.1\%$ . Gamma ray attenuation bulk density measurements were acquired at 2-cm intervals on the whole-round cores using a Geotek multi-sensor core logger; uncertainty of these values is  $\sim 0.075 \text{ g/cm}^3$  based on the standard deviation between repeat measurements on a subset of samples. Depths are reported in meters below sea floor (mbsf). *Morgan et al.* [2017] provide additional details on the core measurements.

## 2.3. Downhole Velocity Measurements

P-wave sonic velocities were measured in open hole at 5-cm spacing with a source frequency of 6 kHz (wavelength of  $\sim 50 \text{ cm}$  at 3000 m/s) throughout the entire drill hole using a wireline logging tool. Uncertainties for the downhole sonic velocities are estimated to be  $\sim 250 \text{ m/s}$  based on uncertainties in travel time picks. Vertical seismic profile (VSP) measurements were recorded at 1.25-5.0 m spacing throughout the drill hole using a 30/30 cubic inch Sercel Mini GI air gun source (wavelength of  $\sim 30 \text{ m}$  for a frequency of 100 Hz and velocity of 3000 m/s). P-wave velocities from the VSP were calculated using procedures developed in *Schmitt et al.* [2007], and have an estimated uncertainty of  $\sim 85 \text{ m/s}$ . Downhole depths were calculated from wireline distance, and have been corrected to mbsf for consistency. Additional details on the downhole velocity measurements are provided in *Morgan et al.* [2017].

### 3. Results

#### 3.1. Hole M0077A Physical Properties

Figure 3 summarizes velocity, porosity, and density measurements for the cored interval of Hole M0077A (505.7-1334.7 mbsf), and average values for each lithological subunit are given in Table 1. Porosity trends are typically observed to be inversely correlated with velocity, while density trends are positively correlated with velocity. Discrete sample velocities at most depths are consistently slightly higher than downhole log and VSP velocities. This is likely in part because lower-frequency log and VSP measurements sample fractures at a larger scale (seismic wavelengths of ~50 cm and 30 m, respectively) than the discrete samples (seismic wavelength of ~1 cm), and discrete samples are specifically selected at positions where the core is relatively intact. Overall, changes in velocity with depth are consistent across the three different velocity measurements (Figure 3c).

In the Paleogene (Pg) sedimentary rock, marlstone/limestone-dominated subunits 1A-1D have lower velocities and densities, and higher porosities, than the underlying limestone-dominated subunits 1E-1F (Figure 3 and Table 1). With increasing depth, velocities increase from 2500-3000 m/s to 3000-4000 m/s (Figure 3c), porosities decrease from 25-35% to 10-15% (Figure 3d), and bulk densities increase from ~2.0 g/cm<sup>3</sup> to 2.5 g/cm<sup>3</sup> (Figure 3e). A core photograph of representative limestone from unit 1F, near the base of the Pg sedimentary rock, is displayed in Figure 4a. There is a remarkable decrease in velocities and bulk densities, and a prominent increase in porosities, at the boundary between Pg sedimentary rock (unit 1) and suevite (unit 2) at ~617 mbsf.

The suevite (unit 2, Figures 4b-d) consists of clasts of impact melt, sedimentary rock, and basement lithologies, embedded in a fine-grained dominantly calcitic matrix, with maximum clast size increasing with depth from 0.2-1.0 cm to >20-25 cm [Morgan *et al.*, 2017]. Suevite discrete sample measurements of velocities, porosities, and densities display an increase in variability at depths >678 mbsf (Figure 3). Velocities are ~2800-3300 m/s in the suevite from ~617 to 706 mbsf, where a sharp increase in borehole sonic P-wave values is observed to



average velocities of ~3700 m/s (Figure 3c). This velocity increase correlates at 706 mbsf with the first observation of significant impact melt rock as up to 60-cm-thick intercalations in suevite, and with an increase in average maximum clast size from ~5 cm to ~13 cm in its host suevite [Morgan *et al.*, 2017]. This velocity increase is also close to the boundary between subunits 2B and 2C at 713 mbsf, which is characterized by a change in suevite color from green, gray, and black in subunit 2B (Figure 4c) to brown in subunit 2C (Figure 4d). Suevite porosities decrease from ~35% at 617 mbsf to ~31% at 706 mbsf, with a sharp decrease to values of ~20% in the lowermost part (706-722 mbsf) of the unit. Suevite bulk densities increase with depth from 2.0-2.1 g/cm<sup>3</sup> in unit 2A (617-665 mbsf) to 2.3-2.4 g/cm<sup>3</sup> in unit 2C (713-722 mbsf). Near the base of unit 2B from ~689-706 mbsf a decrease in sample and logging velocities (from ~3100-3300 m/s to ~2800-2850 m/s), a decrease in densities (from ~2.2 g/cm<sup>3</sup> to ~2.15 g/cm<sup>3</sup>), and an increase in porosities (from ~26% to ~31%) is observed for the suevite (Figure 3). Additional analyses will be required to explain these observations as our visual inspection of the core provides no clear reason for the change in physical properties from 689-706 mbsf.

Impact melt rock (Figure 4e and Table 1, units 3A-3B) velocities (3600-4400 m/s), densities (2.29-2.37 g/cm<sup>3</sup>), and porosities (19-22%) are similar to the suevite at 706-722 mbsf. Crystalline basement unit 4 is not divided into subunits by Morgan *et al.* [2017]. The dominant lithology is granitoid, but significant suevite, impact melt rock, and dolerite rock types are also identified, and physical property values display increased variability at depths 1251-1316 mbsf where suevite and impact melt rock are prevalent (Figure 3). Velocities in unit 4 are typically 4000-4200 m/s, but higher velocities averaging 4821 m/s are observed for discrete sample measurements of dolerite (Figure 3 and Table 1). Densities are significantly lower (2.28-2.33 g/cm<sup>3</sup> vs. 2.40-2.58 g/cm<sup>3</sup>) and porosities significantly higher (15-19% vs. 10%) for suevite and impact melt rock compared to granitoid and dolerite rocks (Figure 3 and Table 1). Compared to units 2 and 3, the suevite and impact melt rock within unit 4 have higher velocities and densities, and lower porosities (Figure 3 and Table 1).

### 3.2. Integration of Expedition 364 Data with Surface Seismic Datasets

Figure 5 compares the downhole sonic log and VSP with seismic reflection images from three profiles, all within 200 m of Hole M0077A (Figure 1c); we converted the seismic reflection data to depth using the 1D VSP velocity profile at the drill site. The different methods sample the subsurface at different seismic wavelengths: ~50 cm, ~30 m, and ~150 m at peak ring depths for downhole sonic, VSP, and seismic reflection, respectively. The Pg sedimentary rock is associated with a subhorizontal layered reflective sequence [e.g., *Morgan et al.*, 1997]. A ~500-m/s increase in VSP velocities at ~300 m depth correlates with a large amplitude reflection on the seismic images, but is above the depths at which core was recovered. The sharp changes in downhole sonic velocities at the top (617 mbsf) and base (706 mbsf) of suevite (Figure 5a) correspond to the top (580-625 m depth) and base (650-690 m depth) of high-amplitude low-frequency reflectors imaged on the seismic reflection profiles (Figure 5b-d). Short, dipping, low-frequency reflectors are imaged in the profiles at depths of ~725-1100 m, likely associated with the impact melt rock and fractured basement. Reflectivity is largely incoherent at depths >1100 m in Figure 5b-d.

Figure 2 places Hole M0077A measurements in the regional context. A ~100-200 m thick layer of low-velocity (~3000-3200 m/s, compared with >3600 m/s above and below) rocks lies at the top of the peak ring in FWI tomographic images [*Morgan et al.*, 2011]. The top of the low-velocity zone correlates with the top of the package of low-frequency reflectors imaged on the seismic reflection data, and tracks the interpreted location of the K-Pg boundary from the top of the peak ring into the annular trough. At Hole M0077A the base of the low-velocity zone in downhole sonic data correlates with the base of the low-frequency reflector package (Figure 5). However, *Morgan et al.* [2011] note that the velocity increase at the base of the low-velocity zone is associated with a deeper intermittent low-frequency reflector. We present both interpretations in Figure 2.

Figure 6 displays the broader context of the seismic reflection profiles of Figure 5. We use the low-velocity zone in the high-resolution FWI velocity models of *Morgan et al.* [2011; e.g.,

Figure 2], where available, as a guide for mapping the suevite. Average suevite thickness is ~130 m in the annular trough, ~200 m in the central basin, and ~100 or ~165 m on the peak ring for the two different interpretations presented in Figure 5. Based on past mapping [Gulick *et al.*, 2013] and onshore boreholes, we interpret the top of the suevite as the K-Pg boundary layer equivalent within the crater; the suevite unit overlies slump blocks and impact melt rock in the annular trough and overlies impact melt rock in the central basin (Figure 6).

## 4. Discussion

### 4.1. Physical Property Changes

Figure 3 illustrates that there is considerable variability in velocity, density, and porosity measurements at Hole M0077A. Factors that might affect the physical properties include composition, fractures (i.e., abundance, connectivity, open, filled with secondary minerals), depositional rate, and intensity of shock. For a given rock type, we expect P-wave velocity to increase, density to increase, and porosity to decrease with increasing depth beneath the seafloor as cracks within the rock close with increasing pressure [e.g., see review in Schmitt, 2015]. Laboratory measurements of sedimentary rock such as limestone yield lower velocity and density values than those of crystalline rock such as granite [e.g., Birch, 1960]. The addition of clay, which could form as an alteration product from fluids associated with a post-impact hydrothermal system, will decrease P-wave velocities; experiments in sandstone show that a very small amount of clay (1%) will significantly reduce the elastic modulus [Han *et al.*, 1986]. Clays typically have lower densities than the material they replace, and thus alteration should also decrease bulk density. Adding cracks to a rock will decrease velocity and density, and increase porosity [Walsh, 1965; Toksöz *et al.*, 1976]. Rapid sedimentary rock deposition is associated with preservation of high porosities if pore fluid pressure is preserved [Bloch *et al.*, 2002]. Experiments show that shock, especially at high temperatures, will reduce the density of quartz [Langenhorst and Deutsch, 1994]. We will consider these factors when discussing the physical property changes observed at the Chicxulub peak ring.

## 4.2. Low-Velocity Zone

A low-velocity zone is observed in downhole sonic, VSP, and FWI velocity measurements (Figure 5a). Spatial resolution is ~80-cm for sonic, ~30-m for VSP, and ~150 m for FWI. As a consequence of resolution differences, the top and bottom of the FWI low-velocity zone is relatively smooth in comparison to the sharp boundaries in the sonic measurements (the VSP measurements are at a scale between sonic and FWI).

The top of the low-velocity zone in FWI data near Hole M0077A is at ~630 mbsf, which is ~13 m deeper than the top of the low-velocity zone at 617 mbsf observed in downhole sonic velocity measurements (Figure 5a). This discrepancy is likely the result of seismic anisotropy. The refracted energy used to construct the FWI velocity model primarily traveled in a horizontal direction, which is typically faster than velocities in the vertical direction in layered sediments. This anisotropy will result in faster velocities above the low-velocity zone in FWI velocity models, and a greater depth to the low-velocity zone.

The base of the low-velocity zone in FWI data near Hole M0077A is at ~800 mbsf, corresponding to intermittent low-frequency reflectivity imaged in surface seismic reflection data, although this depth is also probably overestimated due to anisotropy (Figures 2 and 5; note that Figure 2 is depth below sea level and needs to be shifted up 19.8 m to compare with depth below seafloor plotted in Figure 5). This depth results in an estimated thickness of ~170 m in the FWI model, which is considerably greater than the thickness of ~89 m observed in the sonic velocity log. The FWI velocity model, however, is band-limited, which means that an abrupt-edged low-velocity layer will be spread over a larger distance which can account for some of the thickness differences.

Alternatively, we can use the seismic reflection imaging as a guide for the low-velocity zone. Amplitude changes in seismic reflection data are caused by changes in velocity and density. The top of the low-velocity zone correlates with sharp decreases in both velocity and density (Figure 3), and correlates with the top of a high-amplitude low-frequency reflector package in seismic reflection images (Figure 5). The base of the low-velocity zone in downhole sonic measurements

is associated with a sharp increase in velocity, and a more gradual increase in density, and correlates with the base of the high-amplitude low-frequency reflector package. If we use this interpretation (dashed lines in Figure 5b-d), then the low-velocity zone thickness is ~75-90 m, which is consistent with the downhole sonic measurements. We present both interpretations for low-velocity zone thickness in Figure 6, and plan future work on FWI modeling to better resolve the low-velocity zone thickness throughout the crater.

### 4.3. Onshore Wells

We can compare Hole M0077A physical properties with nearby ICDP well Yaxcopoil-1 (Yax-1) where velocity, porosity, and density measurements were made on discrete samples [Vermeesch and Morgan, 2004; Mayr et al., 2008; Elbra and Pesonen, 2011], and with well Y6 where velocity measurements were made on sparse samples [Morgan et al., 2000; Vermeesch, 2006] (see Figure 1 for well locations). Stratigraphy at Yax-1 consists of Cenozoic sedimentary rock (795 m thick), suevite and brecciated impact melt rock (100 m thick), and Cretaceous sedimentary rock megablocks (616 m thick) [Kring et al., 2004; Stöffler et al., 2004], while Y6 consists of Pg sedimentary rock (~1200 m thick), suevite (~70 m thick), and impact melt rock (~385 m thick) [Hildebrand et al., 1991; Sharpton et al., 1996; Kring, 2005]. The equivalent of the Yax-1 Cretaceous megablocks are interpreted to be down-dropped to >3.5 km depth at Hole M0077A, over two km below the bottom of the borehole [Gulick et al., 2013]. Across the boundary from Pg sedimentary rock to suevite at Yax-1, velocities decrease from ~3700-4100 m/s to ~2800-3500 m/s, porosities increase from ~10-15% to ~18-37%, and bulk densities decrease from ~2.4-2.55 g/cm<sup>3</sup> to ~2.0-2.35 g/cm<sup>3</sup> [Mayr et al., 2008; Elbra and Pesonen, 2011]. Physical properties are relatively constant within units 1-5 (upper 90 m) of the Yax-1 suevite, but change abruptly in “Lower Suevite” unit 6 (lower 10 m, where lithic components are dominated by carbonates) to velocities of 4.0-6.5 km/s, porosities of 1-11%, and densities of 2.35-2.6 g/cm<sup>3</sup> [Mayr et al., 2008; Elbra and Pesonen, 2011]. At Y6 velocities average 4100 m/s, 3900 m/s, and

5800 m/s in the lowermost Pg sedimentary rock, suevite, and impact melt rock, respectively [Morgan *et al.*, 2000; Vermeesch, 2006].

#### 4.4. Suevite

The boundary between Pg sedimentary rock and suevite at 617 mbsf in Hole M0077A is associated with a sharp decrease in downhole sonic log velocity, an increase in porosity, a decrease in bulk density, the top of the low-frequency reflector package on seismic reflection profiles, and the top of a low-velocity layer in FWI images (Figures 2, 3, and 5). Similar velocity, porosity, and density changes at the top of the suevite are observed at onshore well Yax-1 [Mayr *et al.*, 2008; Elbra and Pesonen, 2011] located ~82 km to the south (Figure 1), suggesting that this boundary might be fairly uniform in physical properties throughout the impact basin. An increase in variability in velocity, porosity, and density values at depths >678 mbsf in Hole M0077A (Figure 3) is likely a result of maximum clast size increasing to >5 cm, resulting in sample plugs that may consist entirely of either matrix or a single clast (Figure 4c). The base of the suevite section, identified from core data at 722 mbsf in Hole M0077A, is not associated with a clear change in physical properties; instead, the major change in physical properties (increase in velocity and density, and a decrease in porosity) is observed at ~706 mbsf (Figure 3) where coherent bodies of impact melt rock >10 cm thick first occur. The physical properties (Figure 3) of the lowest part of the suevite (706-722 mbsf) in Hole M0077A (Figure 4d) are similar to those of the underlying impact melt rock units 3A and 3B at 722-747 mbsf (Figure 4e), which suggests that values are dominated by the melt clasts which range in size from a few mm to >10 cm at depths 706-722 mbsf [Morgan *et al.*, 2017].

Suevite from depths 617 to 706 mbsf is characterized by lower velocities and densities, and higher porosities, than the overlying Pg sedimentary rock and underlying suevite and impact melt rock (Figure 3). Decreased P-wave velocity in a material can be caused by the addition of cracks [e.g., Walsh, 1965; Toksöz *et al.*, 1976] or preserved porosity due to rapid emplacement [e.g., Bloch *et al.*, 2002]. However, fractures are not commonly observed in suevite at Hole M0077A

and no significant overpressure was observed [*Morgan et al.*, 2017]. Alteration to clay can also decrease velocities, and suevite in this interval is dominated by rounded, shard-shaped impact melt particles that were produced from highly vesicular, glassy impact melt that is now pervasively altered to phyllosilicates. Some pore space has been filled with secondary zeolites and calcite. Also observed are dark gray subvertical pipes or patches interpreted as possible degassing or dewatering pipes, and vesicular melt rock fragments where vesicles are either empty or filled with carbonate and/or matrix material. Alteration products and gas vesicles were also documented in suevite at onshore borehole Yax-1, where analyses show that early Ca-Na-K metasomatism is followed by abundant phyllosilicate clay replacement [*Hecht et al.*, 2004; *Kring et al.*, 2004; *Zürcher and Kring*, 2004]. Initial analyses and visual inspection at Hole M0077A indicate that most of the former glassy melt has been devitrified to clay minerals within the suevite, while glass in the overlying Paleogene sedimentary rock is either silicified or calcitized with less alteration to clay. We interpret the observed low P-wave velocity and density in the suevite, at depths 617 to 706 mbsf, as a function of their richness in alteration products that are preferentially composed of water-rich, high-porosity phyllosilicates/clay minerals and zeolites. High porosities are also consistent with the observations of pore space, vugs and vesiculated clasts of impact melt in the suevite.

*Wittmann et al.* [2007] propose a suevite emplacement model based on petrologic and image analytical methods of well Yax-1 cores that starts with excavation-flow material interacting with the ejecta plume, followed by lateral transport during central uplift collapse, and finalized by collapse of the ejecta plume, fall back of ejecta, and very minor aquatic reworking. There is also evidence in the uppermost units for gravity flows triggered by ocean water invasion or an impact seismic wave [*Goto et al.*, 2004]. We would expect that excavation flow and lateral mass transport would preferentially fill in and smooth the crater floor, with flow downslope during and after peak-ring formation [*Kring*, 2005]. The later stage of fall back ejecta should drape the lower suevite with relatively constant thickness, with some variability associated with gravity flows. Our mapping of the top and base of the main suevite unit (Figure 6) can help test this

model. In Figure 6a, there are two interpretations for suevite thickness on the peak ring, but with either interpretation the suevite thickens from the peak ring (~100-160 m) into the central basin (~200 m); a thicker suevite in the central basin compared to the top of the peak ring is consistent with observations from onshore boreholes S1 and C1, where suevite thickness is ~400 m and ~200 m, respectively [Hildebrand *et al.*, 1991; Kring, 2005]. Figure 6b is more complex, with the suevite either thickening or thinning from the peak ring (~80-165 m) into the annular trough (~115 m) depending on the interpretation on top of the peak ring. In Figure 6c there is slight thickening of the suevite from the peak ring (~110 m) into the annular trough (~140 m). Regardless of which suevite thickness interpretation is correct on top of the peak ring, our mapping indicates variable suevite thickness which supports a model that includes ground surge and lateral mass transport. The mapping is also consistent with the Kring [2005] model for suevite flowing downslope from a collapsing central uplift during and after peak-ring formation, accumulating preferentially within the central basin (and perhaps also the annular trough). Our mapping implies that, post-impact, suevite covered the entire floor of the impact basin including the annular trough, peak ring, and central basin.

#### **4.5. Impact Melt Rock**

Previous studies have interpreted a low-frequency reflector on seismic reflection profiles, imaged largely within the central basin, as the top of an impact melt sheet [Barton *et al.*, 2010; Morgan *et al.*, 2011; Gulick *et al.*, 2013]. This reflector is correlated with an increase to velocities >5500 m/s, is mapped at an average depth of 1900 m throughout the central basin and discontinuously in the annular trough, and is mostly absent beneath the peak ring [Barton *et al.*, 2010; Morgan *et al.*, 2011; Gulick *et al.*, 2013]. The 25-m-thick impact melt rock unit underlying the suevite at Hole M0077A is at ~722-747 mbsf, much shallower than the expected top of the coherent melt sheet at ~1900 m. Therefore, it probably represents a thin interval of melt deposited on top of the granitoid peak ring. We do interpret a thicker interval of impact melt rock underlying the suevite within the central basin (Figure 6a).



Onshore wells C1, S1, and Y6 (Figure 1) encountered 110 to >360-m-thick impact melt rock at the bottom of the boreholes [Hildebrand *et al.*, 1991; Sharpton *et al.*, 1992; Ward *et al.*, 1995; Kring *et al.*, 2004], which is substantially thicker than drilled at Hole M0077A. Discrete sample measurements on the impact melt rock at well Y6 have velocity values of 5800 m/s and density values of 2.68 g/cm<sup>3</sup> [Morgan *et al.*, 2000; Vermeesch, 2006], which are considerably higher than the mean values of 3788-4144 m/s (downhole sonic log and discrete samples, Table 1) and 2.32-2.34 g/cm<sup>3</sup> (MSCL and discrete samples, Table 1) measured for impact melt rock units 3A and 3B at Hole M0077A. Compared to the suevite and impact melt rock at Hole M0077A, and the suevite in well Y6, the Y6 impact melt rock has much less clay, zeolite, and carbonate alteration products [Kring and Boynton, 1992; Schuraytz *et al.*, 1994]. Fracturing is not common in Hole M0077A impact melt rock [Morgan *et al.*, 2017], so the velocity and density differences between Y6 and M0077A melt rock cannot be explained by the effect of cracks on physical properties. However, as in the suevite, alteration products such as smectite, zeolite, silica, and chloritoid/chlorite, and also vesicles are prevalent in Hole M0077A impact melt rock [Morgan *et al.*, 2017], and these are the likely cause of the observed low velocity, low density, and high porosity.

#### **4.6. Peak Ring Rocks**

Velocities of 4000-4225 m/s are measured in the granitoid rocks at Hole M0077A (Figure 3 and Table 1), which are substantially lower than typical granite velocities of 5400-6000 m/s measured at room temperatures and low pressures [Birch, 1960; Nur and Simmons, 1969; David *et al.*, 1999]. Likewise, densities of 2.39-2.44 g/cm<sup>3</sup> and porosities of 8-13% (Figure 3 and Table 1) significantly differ from typical granite values of 2.62-2.67 g/cm<sup>3</sup> and <1%, respectively [Birch, 1960; Nur and Simmons, 1969]. In comparison, samples from an allochthonous 275-m granitic megablock drilled in the annular moat of the Chesapeake Bay impact structure have velocities, densities, and porosities of 5800-6500 m/s, 2.61-2.66 g/cm<sup>3</sup>, and <1%, respectively [Mayr *et al.*, 2009]; these values largely overlap typical granite values [Birch, 1960; Nur and

369 *Simmons, 1969; David et al., 1999*]. Exterior to the Chicxulub crater rim, velocities of 6000-  
370 6300 m/s are observed at depths of 6-15 km [*Christeson et al., 2001*], which agree well with  
371 laboratory measurements of 6000-6400 m/s for granite at pressures of 2-4 kbar [*Birch, 1960*].  
372 *Morgan et al. [2016]* estimate that material that formed the Chicxulub peak ring originated from  
373 8- to 10-km depth, and moved >20 km during crater formation. Shock metamorphism and  
374 subsequent brecciation during crater excavation and modification decrease the seismic velocity  
375 and density [e.g., *Walsh, 1965; Toksöz et al., 1976; Langenhorst and Deutsch, 1994*]. Fractures  
376 (Figure 4f), foliated shear zones, and cataclasites are observed extensively in the granitoid  
377 section [*Morgan et al., 2016*], and the physical property data presented here suggest that highly  
378 shocked and damaged lithologies are present and pervasive throughout the peak ring.

379 Although the peak ring is predominantly composed of granitoid, other lithologies are  
380 observed in the 588 m cored section of unit 4 including cumulated thicknesses of 46 m of  
381 suevite, 24 m of impact melt rock, and 15 m of dolerite (Figure 3). Both the suevite and impact  
382 melt rock have higher velocities, and lower porosities, than observed in units 2 and 3 (Table 1).  
383 The unit 4 suevite and impact melt rock have no visible carbonate (lower velocity) clasts, but  
384 mafic metamorphic (higher velocity) clasts are present [*Morgan et al., 2017*]. Both suevite and  
385 impact melt rock are pervasively altered, with the clay fraction dominated by phyllosilicates,  
386 mainly mica [*Morgan et al., 2017*]. As for units 2 and 3, the overall low velocities and densities,  
387 and high porosities, of the unit 4 suevite and impact melt rock are attributed to the alteration  
388 products; the higher velocities and lower porosities compared to units 2 and 3 are likely a result  
389 of compositional differences, especially the lack of carbonate clasts.

390 Within crystalline basement unit 4, the suevite and impact melt rock are associated with  
391 higher porosities (15-19%) and lower densities (2.28-2.33 g/cm<sup>3</sup>), and the dolerite with higher  
392 sample and borehole sonic velocities (4821 m/s and 4265 m/s, respectively) and higher densities  
393 (2.57-2.58 g/cm<sup>3</sup>) compared to the granitoid measurements (Figure 3 and Table 1). The increase  
394 in porosity of the suevite and impact melt rock is important, because it implies an increase in  
395 permeability especially in the region between 1251-1316 mbsf dominated by suevite and impact

melt rock (Figure 3). In Yax-1, similar intervals were pathways for circulating hydrothermal fluid [Abramov and Kring, 2007] and that may also be the case in M0077A.

Borehole sonic, VSP, and core determinations of P-wave velocities and densities in the deformed zones of impact structures are rare [Popov *et al.*, 2014]. One useful comparison comes from drilling into the central peak of the Bosumtwi impact crater, a ~10.5 km diameter, 1.07 Ma old complex crater in Ghana [Scholz *et al.*, 2002; Koeberl *et al.*, 2007]. The Bosumtwi target rocks are primarily greenschist facies metasediments; cores and geophysical logs from the ~250 m thick interval down from the top of the central peak revealed an interleaved mixture of polymict and monomict lithic breccias, impact melt-poor suevite, and blocks of target rock reminiscent of Fig. 3a [Ferrière *et al.*, 2007]. MSCL logging [Hunze and Wonik, 2007] and discrete sample measurements [Elbra *et al.*, 2007] also generally show low densities. The VSP P-wave velocities increase with depth by ~30% from 2.6 km/s to 3.34 km/s in the 200-m-thick deformed uplift zone [Schmitt *et al.*, 2007]. These values, too, are substantially less than the ~5.5 km/s expected for the undamaged target metasediments. The rapid changes in P-wave velocity with depth at Bosumtwi relative to those seen at Chicxulub peak ring drilling likely originate from the large differences in the dimensions and material displacement magnitudes between the two structures, although the P-wave velocities reflect in part fracturing and damage within the shifted target rock.

## 5. Conclusions

Chicxulub peak-ring rocks at Hole M0077A have unusual physical properties. Across the boundary between post-impact sedimentary rock and suevite we measure a sharp decrease in velocities and densities, and an increase in porosity. Typical suevite values are 2900-3700 m/s, 2.06-2.37 g/cm<sup>3</sup>, and 20-35% for velocity, density, and porosity, respectively. The suevite is also associated with a low-frequency reflector package on MCS profiles and a low-velocity layer in FWI images. The thin (25 m) impact melt rock unit has velocities of 3650-4350 m/s, densities of 2.26-2.37 g/cm<sup>3</sup>, and porosities of 19-22%; density and porosity values are intermediate between

the overlying suevite and underlying granitoid rocks, while the velocity values are similar to those for the underlying granitic basement. The Hole M0077A impact melt rock velocities and densities are considerably less than values of 5800 m/s and 2.68 g/cm<sup>3</sup> measured at an onshore well Y6 located in the annular trough. We associate the low velocity, low density, and high porosity of suevite and impact melt rock with rapid emplacement, hydrothermal alteration products and observations of pore space, vugs, and vesicles. Granitoid rocks have velocities of 4000-4200 m/s, densities of 2.39-2.44 g/cm<sup>3</sup>, and porosities of 8-13%; these values differ significantly from typical granite which has higher velocities and densities, and porosities <1%. Hole M0077A granitoid peak-ring physical property values indicate considerable fracturing, and are consistent with numerical models for peak-ring formation where the lithologies present within the peak ring represent the most shocked and damaged rocks in an impact basin. We map thicker suevite away from the peak ring, suggesting that this unit flowed downslope from a collapsing central uplift during and after peak-ring formation, accumulating preferentially within the central basin. We interpret suevite below the Paleogene sediments in the annular trough, peak ring, and central basin, implying that, post impact, suevite covered the entire floor of the impact basin.

**Acknowledgements.** We thank captain and crew, drilling team, and technical staff who participated in shipboard and/or shore-based operations, and Tom Hess, Steffen Saustrup, and Penelope Pharr for technical support at UTIG. The European Consortium for Ocean Research Drilling (ECORD) implemented Expedition 364 with funding from the International Ocean Discovery Program (IODP) and the International Continental scientific Drilling Project (ICDP). We thank the reviewers and editor William McKinnon for their constructive comments on an earlier version of this manuscript. Data and samples can be requested from IODP. U.S. participants were supported by the U.S. Science Support Program and NSF grants OCE 1737351, OCE 1736826, OCE 1737087, OCE 1737037, OCE 1736951, and OCE 1737199. J.V.M was funded by NERC, Grant: NE/P005217/1. This is UTIG contribution 3262.

## References

- Abramov, O., and D. A. Kring (2007), Numerical modeling of impact-induced hydrothermal activity at the Chicxulub crater, *Meteorit. Planet. Sci.*, **42**, 93-112, doi: 10.1111/j.1945-5100.2007.tb00220.x.
- Barton, P. J., R. A. F. Grieve, J. V. Morgan, A. T. Surendra, P. M. Vermeesch, G. L. Christeson, S. P. S. Gulick, and M. R. Warner (2010), Seismic images of Chicxulub impact melt sheet and comparison with the Sudbury structure, in *Large Meteorite Impacts and Planetary Evolution IV*, edited by R. L. Gibson and W. U. Reimold, pp. 103-113, Geol. Soc. Amer. Spec. Pap. 465, doi: 10.1130/2010.2465(07).
- Birch, F. (1960), The velocity of compressional waves in rocks to 10 kilobars: 1, *J. Geophys. Res.*, **65**, 1083-1102, doi: 10.1029/JZ065i004p01083.
- Bloch, S., R. H. Lander, and L. Bonnell (2002), Anomalously high porosity and permeability in deeply buried sandstone reservoirs: Origin and predictability, *AAPG Bulletin*, **86**, 301-328.
- Christeson, G. L., Y. Nakamura, R. T. Buffler, J. Morgan, and M. Warner (2001), Deep crustal structure of the Chicxulub impact crater, *J. Geophys. Res.*, **106**, 21751-21769.
- Collins, G. S., J. V. Morgan, P. J. Barton, G. L. Christeson, S. P. S. Gulick, J. Urrutia-Fucugauchi, M. R. Warner, and K. Wünnemann (2008), Dynamic modeling suggests terrace zone asymmetry in the Chicxulub crater is caused by target heterogeneity, *Earth Planet. Sci. Lett.*, **270**, 221-230.
- David, C., B. Menéndez, and M. Darot (1999), Influence of stress-induced and thermal cracking on physical properties and microstructure of La Peyratte granite, *International Journal of Rock Mechanics and Mining Sciences*, **36**, 433-448, doi: 10.1016/S0148-9062(99)00010-8.

472 Elbra, T., A. Kontny, L. J. Pesonen, N. Schleifer, and C. Schell (2007), Petrophysical and  
 473 paleomagnetic data of drill cores from the Bosumtwi impact structure, Ghana, *Meteorit.*  
 474 *Planet. Sci.*, *42*, 829-838, doi: 10.1111/j.1945-5100.2007.tb01078.x.  
 475 Elbra, T., and L. J. Pesonen (2011), Physical properties of the Yaxcopoil-1 deep drill core,  
 476 Chicxulub impact structure, Mexico, *Meteorit. Planet. Sci.*, *46*, 1640-1652, doi:  
 477 10.1111/j.1945-5100.2011.01253.x.  
 478 Ferrière, L., C. Koeberl, and U. Reimold (2007), Drill core LB- 08A, Bosumtwi impact  
 479 structure, Ghana: Petrographic and shock metamorphic studies of material from the central  
 480 uplift, *Meteorit. Planet. Sci.*, *42*, 611-633, doi: doi:10.1111/j.1945-5100.2007.tb01064.x.  
 481 Goto, K., R. Tada, E. Tajika, T. J. Bralower, T. Hasegawa, and T. Matsui (2004), Evidence for  
 482 ocean water invasion into the Chicxulub Crater at the Cretaceous/Tertiary boundary,  
 483 *Meteorit. Planet. Sci.*, *39*, 1233-1247.  
 484 Grieve, R. A. F., P. B. Robertson, and M. R. Dence (1981), Constraints on the formation of ring  
 485 impact structures, based on terrestrial data, *Proc. Lunar Planet. Sci.*, *12A*, 37-57.  
 486 Gulick, S. P. S., P. J. Barton, G. L. Christeson, J. V. Morgan, M. McDonald, K. Mendoza-  
 487 Cervantes, Z. F. Pearson, A. Surendra, J. Urrutia-Fucugauchi, P. M. Vermeesch, and M. R.  
 488 Warner (2008), Importance of pre-impact crustal structure for the asymmetry of the  
 489 Chicxulub impact crater, *Nature Geosci.*, *1*, 131-135, doi: 10.1038/ngeo103.  
 490 Gulick, S. P. S., G. L. Christeson, P. J. Barton, R. A. F. Grieve, J. V. Morgan, and J. Urrutia-  
 491 Fucugauchi (2013), Geophysical characterization of the Chicxulub impact crater, *Rev.*  
 492 *Geophys.*, *51*, 31-52, doi: 10.1002/rog.200007.  
 493 Han, D.-h., A. Nur, and D. Morgan (1986), Effects of porosity and clay content on wave  
 494 velocities in sandstones, *Geophysics*, *51*, 2093-2107, doi: 10.1190/1.1442062.

495 Hecht, L., A. Wittmann, R. T. Schmitt, and D. Stöffler (2004), Composition of impact melt  
 496 particles and the effects of post- impact alteration in suevitic rocks at the Yaxcopoil- 1 drill  
 497 core, Chicxulub crater, Mexico, *Meteorit. Planet. Sci.*, *39*, 1169-1186, doi:  
 498 doi:10.1111/j.1945-5100.2004.tb01135.x.

499 Hildebrand, A. R., G. T. Penfield, D. A. Kring, M. Pilkington, A. Camargo, Z., S. B. Jacobsen,  
 500 and W. V. Boynton (1991), Chicxulub Crater: A possible Cretaceous/Tertiary boundary  
 501 impact crater on the Yucatán Peninsula, Mexico, *Geology*, *19*, 867-871.

502 Hunze, S., and T. Wonik (2007), Lithological and structural characteristics of the Lake  
 503 Bosumtwi impact crater, Ghana: Interpretation of acoustic televiwer images, *Meteorit.*  
 504 *Planet. Sci.*, *42*, 779-792, doi: 10.1111/j.1945-5100.2007.tb01074.x.

505 Koeberl, C., B. Milkereit, J. T. Overpeck, C. A. Scholz, P. Y. O. Amoako, D. Boamah, S. K.  
 506 Danuor, T. Karp, J. Kueck, R. E. Hecky, J. King, and J. A. Peck (2007), An international and  
 507 multidisciplinary drilling project into a young complex impact structure: The 2004 ICDP  
 508 Bosumtwi impact crater, Ghana, drilling project – An overview, *Meteorit. Planet. Sci.*, *42*,  
 509 483-511.

510 Kring, D. A., and W. V. Boynton (1992), Petrogenesis of an augite-bearing melt rock in the  
 511 Chicxulub structure and its relationship to K/T impact spherules in Haiti, *Nature*, 141-144,  
 512 doi: 10.1038/358141a0.

513 Kring, D. A., F. Hörz, L. Zurcher, and J. U. Fucugauchi (2004), Impact lithologies and their  
 514 emplacement in the Chicxulub impact crater: Initial results from the Chicxulub Scientific  
 515 Drilling Project, Yaxcopoil, Mexico, *Meteorit. Planet. Sci.*, *39*, 879-897, doi:  
 516 10.1111/j.1945-5100.2004.tb00936.x.

517 Kring, D. A. (2005), Hypervelocity collisions into continental crust composed of sediments and  
 518 an underlying crystalline basement: comparing the Ries (~24 km) and Chicxulub (~180 km)  
 519 impact craters, *Chem Erde-Geochem*, 65, 1-46.

520 Langenhorst, F., and A. Deutsch (1994), Shock experiments on pre-heated  $\alpha$ - and  $\beta$ -quartz: I.  
 521 Optical and density data, *Earth Planet. Sci. Lett.*, 125, 407-420, doi: 10.1016/0012-  
 522 821X(94)90229-1.

523 Mayr, S. I., A. Wittmann, H. Burkhardt, Y. Popov, R. Romushkevich, I. Bayuk, P. Heidinger,  
 524 and H. Wilhelm (2008), Integrated interpretation of physical properties of rocks of the  
 525 borehole Yaxcopoil-1 (Chicxulub impact structure), *J. Geophys. Res.*, 113, B07201, doi:  
 526 10.1029/2007JB005420.

527 Mayr, S. I., H. Burkhardt, Y. Popov, R. Romushkevich, D. Miklashevskiy, D. Gorobtsov, P.  
 528 Heidinger, and H. Wilhelm (2009), Physical rock properties of the Eyreville core,  
 529 Chesapeake Bay impact structure, *Geological Society of America Special Papers*, 458, 137-  
 530 163, doi: 10.1130/2009.2458(07).

531 Morgan, J. V., M. R. Warner, J. Brittan, R. Buffler, A. Camargo, G. Christeson, P. Denton, A.  
 532 Hildebrand, R. Hobbs, H. Macintyre, G. Mackenzie, P. Maguire, Marin, Y. Nakamura, M.  
 533 Pilkington, V. Sharpton, D. Snyder, G. Suarez, and A. Trejo (1997), Size and morphology of  
 534 the Chicxulub impact crater, *Nature*, 390, 472-476.

535 Morgan, J. V., M. R. Warner, G. S. Collins, H. J. Melosh, and G. L. Christeson (2000), Peak-ring  
 536 formation in large impact craters: Geophysical constraints from Chicxulub, *Earth Planet. Sci.*  
 537 *Lett.*, 183, 347-354.

538 Morgan, J. V., G. L. Christeson, and C. A. Zelt (2002), Testing the resolution of a 3D velocity  
 539 tomogram across the Chicxulub crater, *Tectonophysics*, 355, 215-226.



540 Morgan, J. V., M. R. Warner, G. S. Collins, R. A. F. Grieve, G. L. Christeson, S. P. S. Gulick,  
 541 and P. J. Barton (2011), Full waveform tomographic images of the peak ring at the Chicxulub  
 542 impact crater, *J. Geophys. Res.*, *116*, B06303, doi: 10.1029/2011JB008210.

543 Morgan, J. V., S. P. S. Gulick, T. Bralower, E. Chenot, G. L. Christeson, P. Claeys, C. S.  
 544 Cockell, G. S. Collins, M. Coolen, L. Ferrière, C. Gebhardt, K. Goto, H. Jones, D. A. Kring,  
 545 E. Le Ber, J. Lofi, X. Long, C. Lowery, C. Mellet, R. Ocampo-Torres, G. R. Osinski, L.  
 546 Perez-Cruz, A. Pickersgill, M. Pölchau, A. Rae, C. Rasmussen, M. Rebolledo-Vieyra, U.  
 547 Riller, H. Sato, D. Schmitt, J. Smit, S. Tikoo-Schantz, N. Tomioka, J. Urrutia-Fucugauchi,  
 548 M. T. Whalen, A. Wittmann, K. Yamaguchi, and W. Zylberman (2016), The formation of  
 549 peak rings in large impact craters, *Science*, *354*, 878-882, doi: 10.1126/science.aah6561.

550 Morgan, J. V., S. P. S. Gulick, C. L. Mellet, S. L. Green, and Expedition 364 Scientists (2017),  
 551 *Chicxulub: Drilling the K-Pg Impact Crater, Proceedings of the International Ocean*  
 552 *Discovery Program, 364*, International Ocean Discovery Program, College Station, TX, doi:  
 553 10.14379/iodp.proc.364.103.2017.

554 Nur, A., and G. Simmons (1969), The effect of saturation on velocity in low porosity rocks,  
 555 *Earth Planet. Sci. Lett.*, *7*, 183-193, doi: 10.1016/0012-821X(69)90035-1.

556 Popov, Y., S. Mayr, R. Romushkevich, H. Burkhardt, and H. Wilhelm (2014), Comparison of  
 557 petrophysical properties of impactites for four meteoritic impact structures, *Meteorit. Planet.*  
 558 *Sci.*, *49*, 896-920, doi: 10.1111/maps.12299.

559 Schmitt, D. R., B. Milkereit, T. Karp, C. Scholz, S. Danuor, D. Meillieux, and M. Welz (2007),  
 560 In situ seismic measurements in borehole LB-08A in the Bosumtwi impact structure, Ghana:  
 561 Preliminary interpretation, *Meteorit. Planet. Sci.*, *42*, 755-768, doi: 10.1111/j.1945-  
 562 5100.2007.tb01072.x.

563 Schmitt, D. R. (2015), 11.03 - Geophysical Properties of the Near Surface Earth: Seismic  
 564 Properties, in *Treatise on Geophysics (Second Edition)*, edited by G. Schubert, pp. 43-87,  
 565 Elsevier, Oxford, doi: 10.1016/B978-0-444-53802-4.00190-1.

566 Scholz, C. A., T. Karp, K. M. Brooks, B. Milkereit, P. Y. O. Amoako, and J. A. Arko (2002),  
 567 Pronounced central uplift identified in the Bosumtwi impact structure, Ghana, using  
 568 multichannel seismic reflection data, *Geology*, 30, 939-942.

569 Schuraytz, B. C., V. L. Sharpton, and L. E. Marín (1994), Petrology of impact-melt rocks at the  
 570 Chicxulub multiring basin, Yucatán, Mexico, *Geology*, 22, 868-872.

571 Sharpton, V. L., G. B. Dalrymple, L. E. Marin, G. Ryder, B. C. Schuraytz, and J. Urrutia-  
 572 Fucugauchi (1992), New links between the Chicxulub impact structure and the  
 573 Cretaceous/Tertiary boundary, *Nature*, 359, 819-821.

574 Sharpton, V. L., L. E. Marín, C. Carney, S. Lee, G. Ryder, B. C. Schuraytz, P. Sikora, and P. D.  
 575 Spudis (1996), A model of the Chicxulub impact basin based on evaluation of geophysical  
 576 data, well logs, and drill core samples, in *The Cretaceous-Tertiary event and other*  
 577 *catastrophes in Earth history*, vol. Geol. Soc. Am., Spec. Pap. 307, edited by G. Ryder, D.  
 578 Fastovsky and S. Gartner, pp. 55-74.

579 Stöffler, D., N. A. Artemieva, B. A. Ivanov, L. Hecht, T. Kenkmann, R. T. Schmitt, R. A. Tagle,  
 580 and A. Wittmann (2004), Origin and emplacement of the impact formation at Chicxulub,  
 581 Mexico, as revealed by the ICDP deep drilling at Yaxcopoil-1 and by numerical modeling,  
 582 *Meteorit. Planet. Sci.*, 39, 1035-1067.

583 Stöffler, D., and R. A. F. Grieve (2007), Impactites, in *Metamorphic Rocks: A Classification and*  
 584 *Glossary of Terms*, edited by D. Fettes and J. Desmons, pp. 82-92, Cambridge University  
 585 Press, Cambridge, UK.

586 Toksöz, M., C. Cheng, and A. Timur (1976), Velocities of seismic waves in porous rocks,  
587 *Geophysics*, *41*, 621-645, doi: 10.1190/1.1440639.

588 Vermeesch, P. M., and J. V. Morgan (2004), Chicxulub central crater structure: Initial results  
589 from physical property measurements and combined velocity and gravity modeling, *Meteorit.*  
590 *Planet. Sci.*, *39*, 1019-1034.

591 Vermeesch, P. M. (2006), Geophysical modelling of the Chicxulub crater, Ph.D. thesis, 418 pp,  
592 Imperial College, London.

593 Virieux, J., and S. Operto (2009), An overview of full-waveform inversion in exploration  
594 geophysics, *Geophysics*, *74*, WCC1-26, doi: 10.1190/1.3238367.

595 Walsh, J. B. (1965), The effect of cracks on the compressibility of rock, *J. Geophys. Res.*, *70*,  
596 381-389, doi: 10.1029/JZ070i002p00381.

597 Ward, W. C., G. Keller, W. Stinnesbeck, and T. Adatte (1995), Yucatán subsurface stratigraphy:  
598 Implications and constraints for the Chicxulub impact, *Geology*, *23*, 873-876.

599 Wittmann, A., T. Kenkmann, L. Hecht, and D. Stöffler (2007), Reconstruction of the Chicxulub  
600 ejecta plume from its deposits in drill core Yaxcopoil-1, *Geol. Soc. Am. Bull.*, *119*, 1151-  
601 1167, doi: 10.1130/B26116.1.

602 Yilmaz, O. (1987), *Seismic Data Processing*, 526 pp., Society of Exploration Geophysics, Tulsa,  
603 OK.

604 Zürcher, L., and D. A. Kring (2004), Hydrothermal alteration in the core of the Yaxcopoil-1  
605 borehole, Chicxulub impact structure, Mexico, *Meteorit. Planet. Sci.*, *39*, 1199-1221, doi:  
606 10.1111/j.1945-5100.2004.tb01137.x.

607  
608

**Table 1.** Average Physical Property Values and Standard Deviation

Subunit	Top Depth (mbsf)	Dominant Lithology	Sample Velocity (m/s)	Sonic Velocity (m/s)	VSP Velocity (m/s)	Sample Porosity (%)	Sample Density (g/cm <sup>3</sup> )	MSCL Density (g/cm <sup>3</sup> )
1A	505.70	marlstone	3147±501	2574±220	2619±33	28±7	2.02±0.08	1.99±0.12
1B	530.18	marlstone limestone	2984±204	2728±211	2642±5	29±5	1.96±0.11	2.07±0.13
1C	537.80	marlstone limestone	3163±404	2680±182	2613±27	28±5	2.05±0.08	2.10±0.13
1D	559.75	marlstone limestone	3101±305	2642±247	2614±62	26±5	2.04±0.13	2.06±0.18
1E	580.89	limestone	3769±392	3159±336	3040±144	21±7	2.28±0.15	2.32±0.16
1F	607.27	limestone	3018±243	3401±300	3082±70	14±2	2.47±0.03	2.37±0.16
1G	616.58	mud-wackestone		3703±107				2.53±0.06
2A	617.33	suevite	3106±126	2921±91	2873±77	35±2	2.06±0.03	2.09±0.07
2B	664.52	suevite	3396±431	3100±255	3187±199	29±7	2.18±0.13	2.17±0.15
2C	712.84	suevite	3635±250	3635±116	3689±25	20±4	2.36±0.08	2.37±0.16
3A	721.61	impact melt rock	4361±361	3878±186	3793±41	19±3	2.37±0.05	2.36±0.16
3B	737.56	impact melt rock	3829±679	3636±188	3898±24	22±4	2.29±0.05	2.26±0.10
4	747.02	granitoid	4171±569	4014±277	4225±134	11±4	2.44±0.07	2.39±0.12
4*	*	suevite	4165±472	3967±308	4103±6	19±6	2.33±0.09	2.30±0.12
4*	*	impact melt rock	4487±550	4014±356	4096±26	15±5	2.33±0.05	2.28±0.15
4*	*	granitoid	4139±569	4006±262	4227±133	10±3	2.46±0.05	2.40±0.10
4*	*	dolerite	4821±335	4265±276	4237±130	10±3	2.57±0.07	2.58±0.22

\*Unit 4 was not divided into subunits; these values are calculated for depths within Unit 4 where core description identified the dominant lithology.

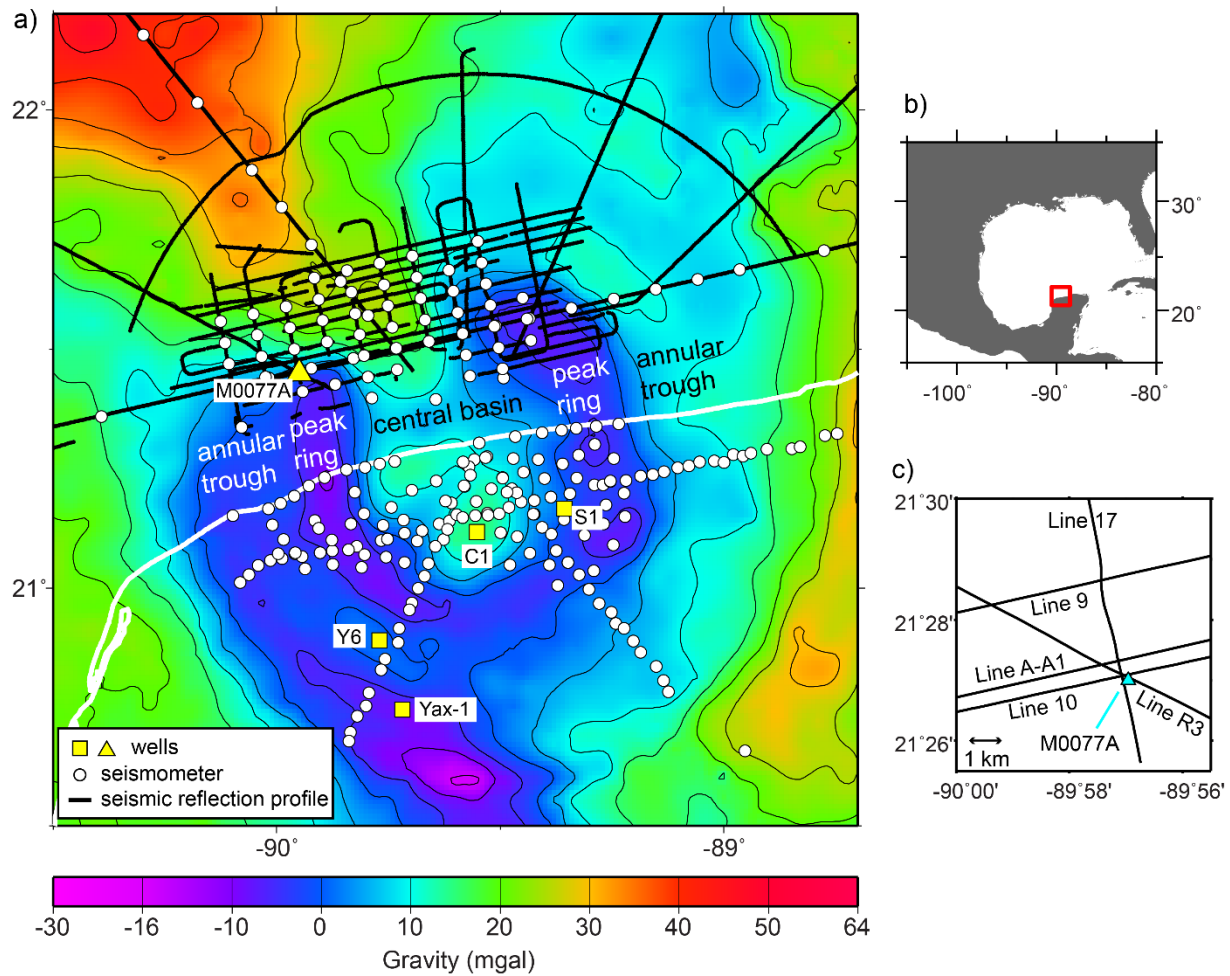


**Figure 1.** a) Bouguer gravity anomaly map (gravity data courtesy of A. Hildebrand and M. Pilkington) over the Chicxulub impact crater. The coastline is displayed with the white line. b) Regional setting, with red rectangle outline the region shown in panel a. c) Close-up of Hole M0077A location showing position of well with respect to seismic profiles. At the closest position to Hole M0077A, Line R3 is 69 m north-northeast, Line 10 is 151 m north, and Line 17b is 161 m west.

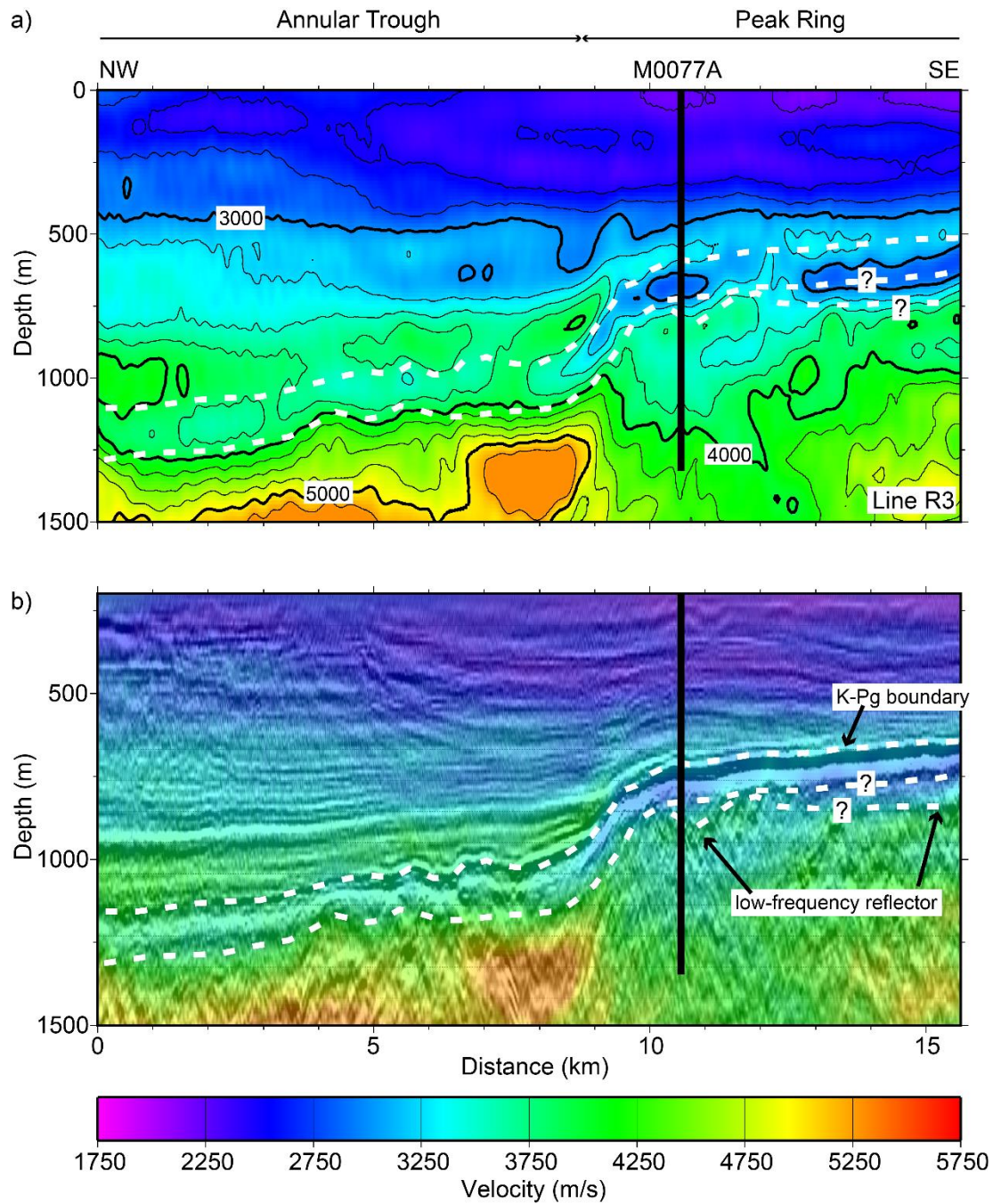


**Figure 2.** Full wavefield inverted velocity model for Line R3 [Morgan *et al.*, 2011]: a) Plotted with a contour interval 250 m/s; b) Overlain on seismic Line R3, with seismic data converted to depth using the same velocity model. White dashed lines mark top and base of low-velocity layer as guided by seismic reflectors; two possible interpretations are shown for base of low-velocity layer within the peak ring.

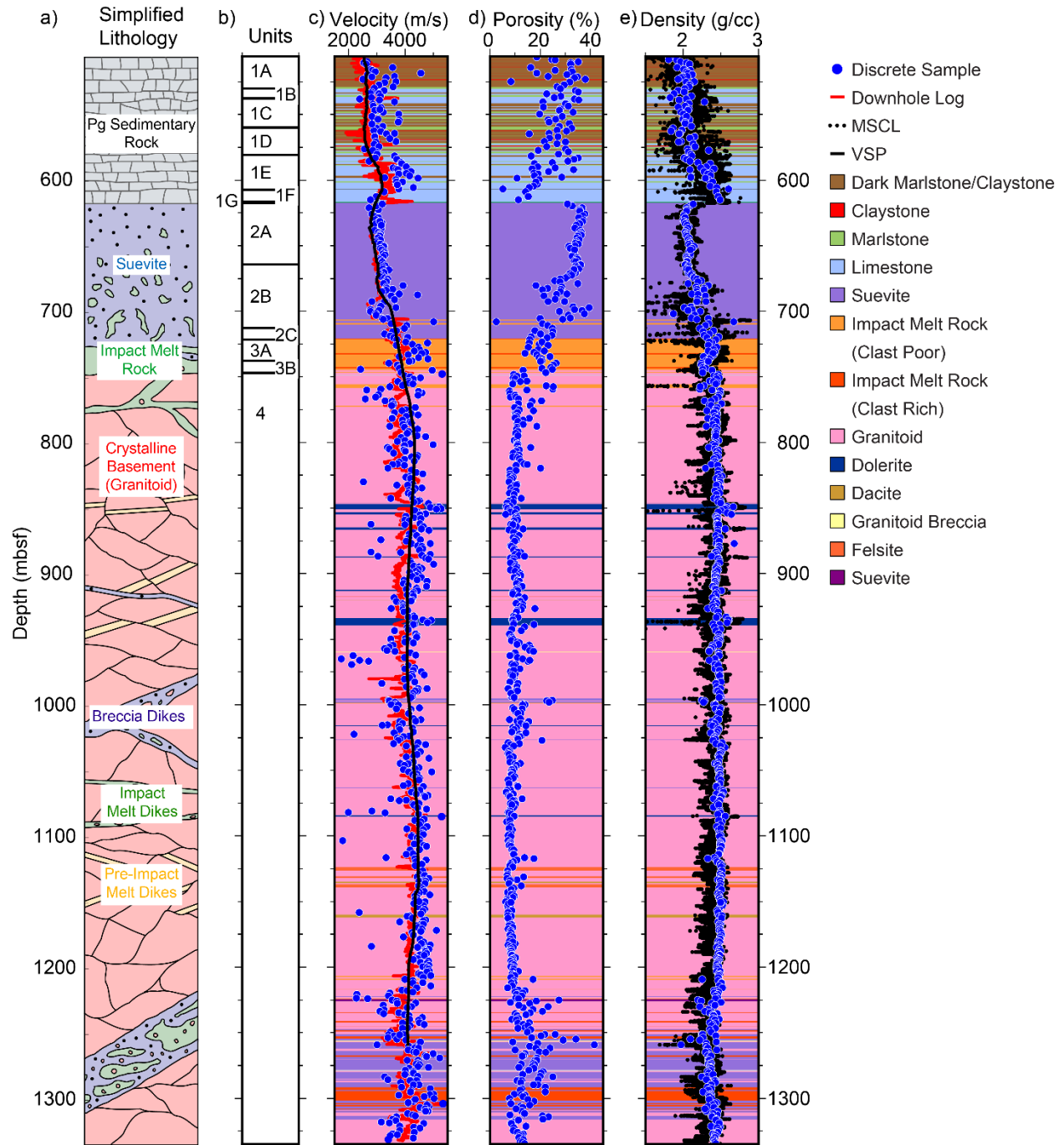


**Figure 3.** Hole M0077A a) Simplified lithology [Morgan *et al.*, 2016]. b) Lithologic unit boundaries [Morgan *et al.*, 2017]. c) P-wave velocity measurements from discrete samples, downhole logging, and vertical seismic profiles (VSP). d) Porosity measurements from discrete samples. e) Bulk density measurements from discrete samples and multi-sensor core logger (MSCL). Detailed lithology plotted as background colors in panels c-e are from Morgan *et al.* [2017].



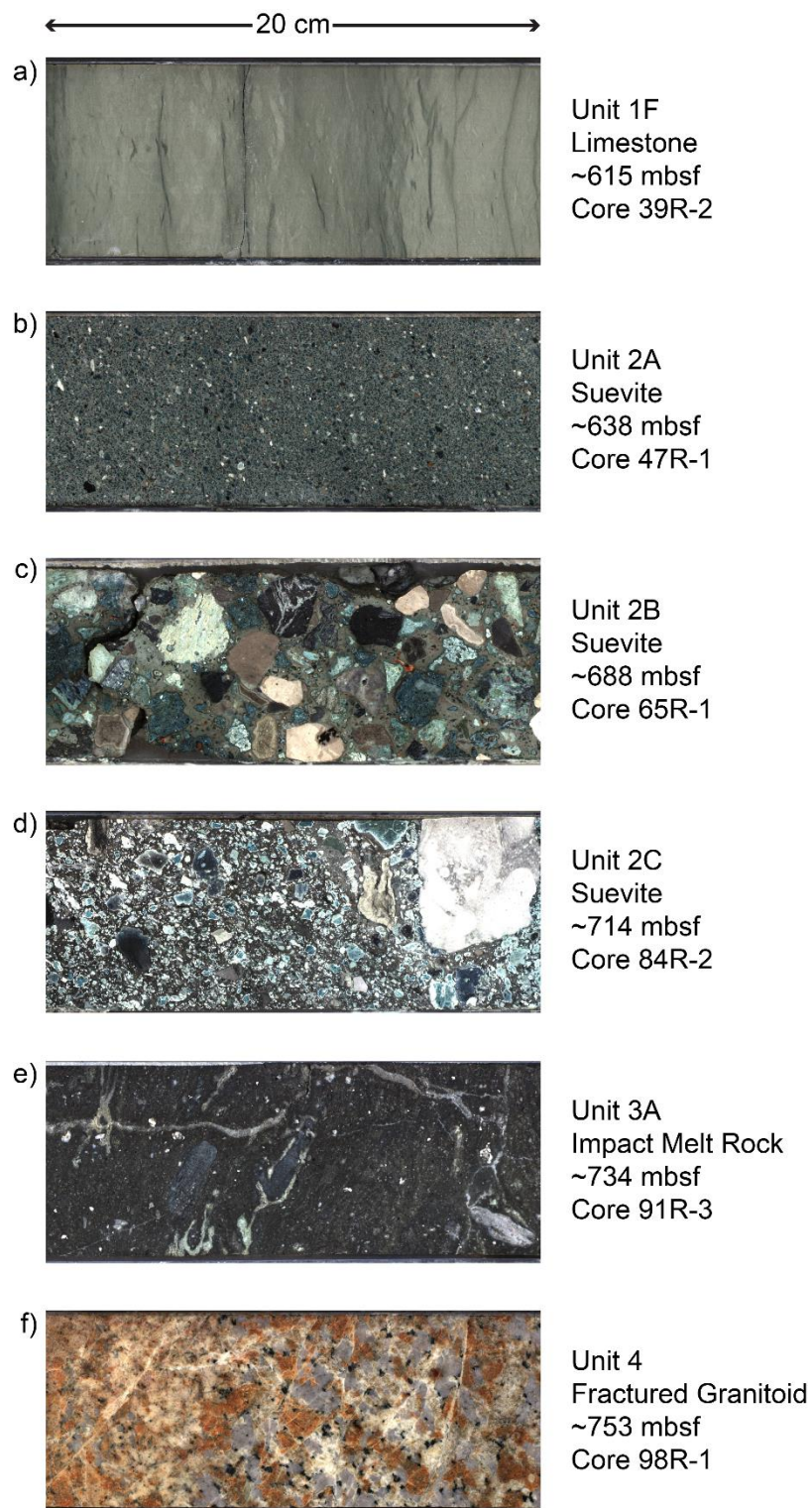


**Figure 4.** Digital line-scan images of the split cores displaying representative limestone, suevite, impact melt rock, and fractured granitoid.



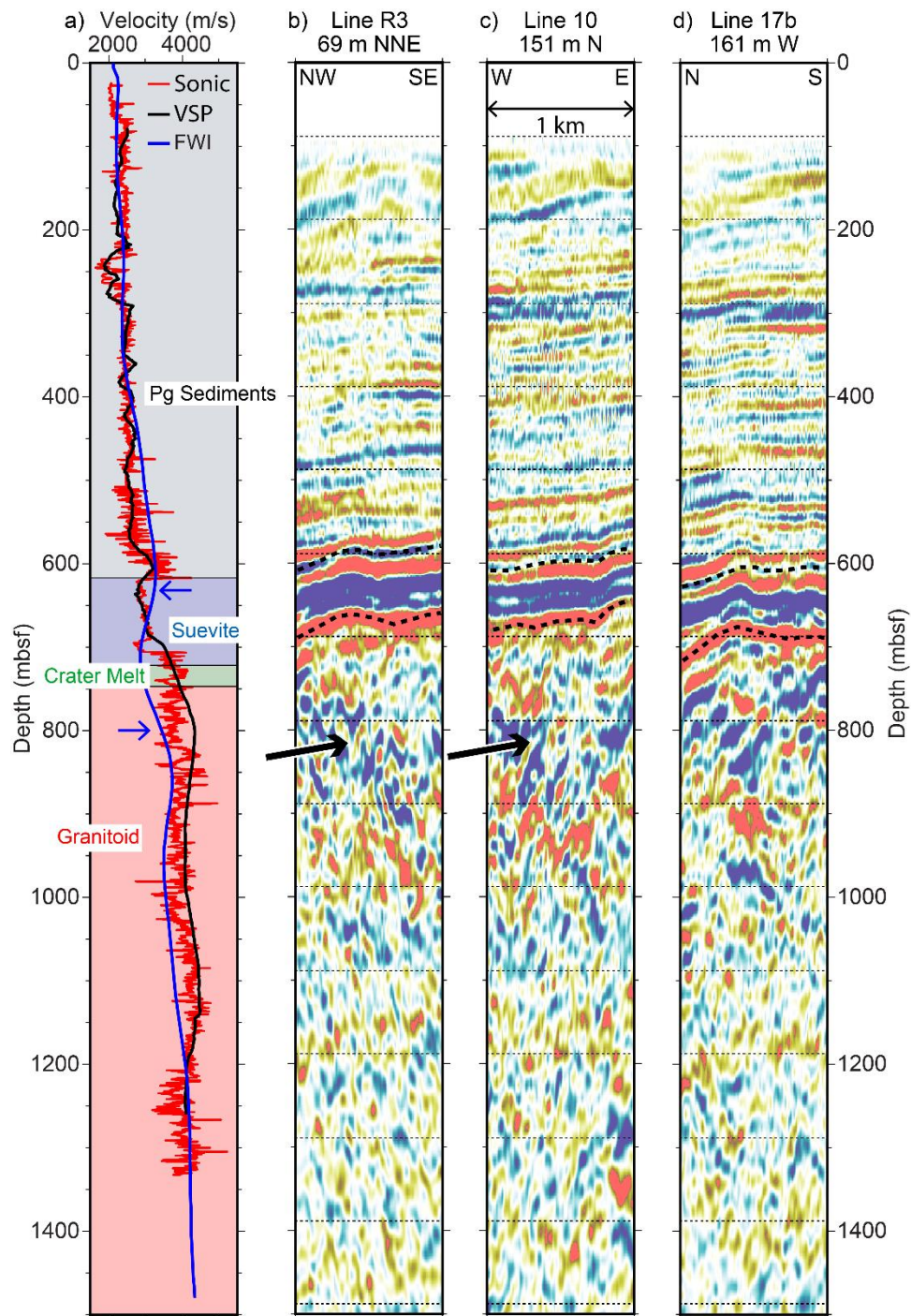


**Figure 5.** a) Comparison of P-wave velocity functions at Hole M0077A. Sonic and VSP are from downhole measurements. FWI is full wavefield inversion for Line R3 [Morgan *et al.*, 2011] shifted from the sea surface to the seafloor at 19.8 m depth; blue arrows point to top and base of a low-velocity zone. Background colors display simplified lithology. b) Line R3, c) Line 10, d) Line 17b seismic images, converted to depth using the 1D Hole M0077A VSP velocity profile, centered at the position closest to Hole M0077A, and shifted 13.3 m to account for water column between source and receivers and seafloor. Locations of the seismic profiles with respect to Hole M0077A are displayed in Figure 1c. Dashed black line shows the interpreted top and base of the suevite unit as mapped in Figure 6, and black arrows point to intermittent low-frequency reflector correlated with the base of the FWI low-velocity layer.

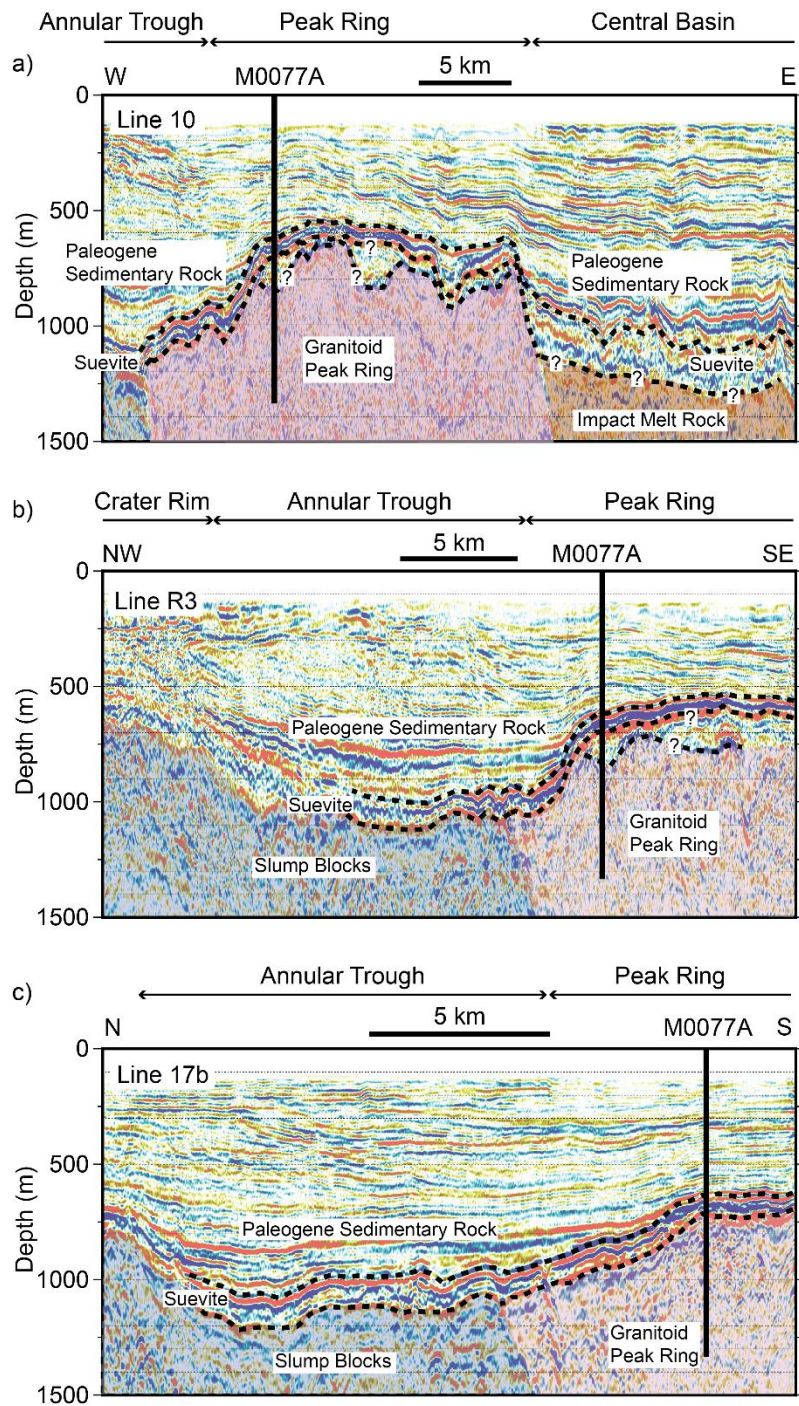


**Figure 6.** Seismic reflection profiles converted to depth using the 1D Hole M0077A VSP velocity profile. Upper dashed line is the interpreted base of the post-impact section, and thus the equivalent of the crater floor post-impact. The lower dashed line is the base of the suevite, with two possible interpretations on the peak ring. Blue shading are slump blocks, pink shading are granitoids of peak ring capped by impact melt rock, and orange shading is potential area of thickened impact melt rock beneath the central basin. a) Line 10; vertical exaggeration (V.E.) ~12.5:1. b) Line R3; V.E. ~10:1. c) Line 17b; V.E. ~6.5:1. Locations of the seismic profiles with respect to Hole M0077A are displayed in Figure 1c.

